First-principles study of metal adatom adsorption on graphene

Kevin T. Chan,[1,2] J. B. Neaton,[3] and Marvin L. Cohen[1,2]
[1]*Department of Physics, University of California, Berkeley, California 94720, USA*
[2]*Materials Sciences Division, Lawrence Berkeley National Laboratory, Berkeley, California 94720, USA*
[3]*The Molecular Foundry, Lawrence Berkeley National Laboratory, Berkeley, California 94720, USA*
(Received 30 April 2008; published 20 June 2008)

The adsorption of 12 different metal adatoms on graphene is studied using first-principles density-functional theory with the generalized gradient approximation. The adsorption energy, geometry, density of states (DOS), dipole moment, and work function of each adatom-graphene system are calculated. For the adatoms studied from groups I–III of the Periodic Table, the results are consistent with ionic bonding, and the adsorption is characterized by minimal change in the graphene electronic states and large charge transfer. For transition, noble, and group IV metals, the calculations are consistent with covalent bonding, and the adsorption is characterized by strong hybridization between adatom and graphene electronic states. For ionically bonded adatoms, the charge transfer is calculated quantitatively using two methods, one based on the DOS and the other based on the real-space-charge density. A variation in dipole moments and work-function shifts across the different adatoms is observed. In particular, the work-function shift shows a general correlation with the induced interfacial dipole of the adatom-graphene system and the ionization potential of the isolated atom.

DOI: 10.1103/PhysRevB.77.235430 PACS number(s): 73.22.−f, 68.43.Bc, 73.63.−b, 73.20.Hb

I. INTRODUCTION

Graphene and carbon nanotubes (CNTs) are among the most prominent nanoscale materials currently studied. The confinement to one or two dimensions and the high symmetry of these materials lead to interesting new physics and many potential applications, especially involving the electronic structure and transport properties. One-dimensional CNTs can be metallic or semiconducting, depending on chirality, and can act as quantum wires with minimal scattering.[1] Two-dimensional (2D) graphene has a rather unique sublattice symmetry and is a zero-gap semiconductor with a pointlike Fermi surface and a linear dispersion at the Fermi level. These properties are responsible for the observed ballistic transport, Dirac-type quasiparticles, and anomalous quantum Hall effects in graphene.[2]

Because of the diversity of properties of the metallic elements, the variety of structures formed, and the availability of experimental techniques at the nanolevel, the adsorption of metals on the surfaces of these systems is a promising approach to controllably modify graphene and CNTs. Adsorption of alkali atoms has been used to chemically dope CNTs (Refs. 3 and 4) and fabricate field effect transistors.[5] Potassium has also been used to chemically dope graphene, allowing graphene quasiparticle dynamics[6] and minimum conductivity[7] to be studied. Furthermore, K atoms have also been used to tune the electronic structure of graphene bilayers.[8]

Metals adsorbed on nanoscale carbon surfaces have been shown experimentally to form a variety of structures, such as continuous coatings or discrete clusters,[9] and these structures can be manipulated to give rise to interesting new phenomena. For example, experiments have demonstrated the ability to control metal adatom diffusion between metal clusters on CNT surfaces.[10] Moreover, understanding the metallic structures that form and their interface with the carbon surface is essential to fabricating electronic devices for applications and transport experiments. Significant progress has been made in recent studies to understand such metal contacts to nanotubes and graphene.[11,12]

Much previous theoretical work on this subject has focused on the adsorption properties of one or a small set of metal adatoms on carbon nanostructures, particularly the structure, bonding, and charge transfer of 2D alkali adatom layers on graphite.[13] Other calculations surveyed of a range of adatoms on single-walled CNTs and reported on trends in binding energy and bond character, as well as the possibility of magnetic adatoms.[14] While there is a close relation between CNTs and graphene, the strong curvature of small-radius CNTs leads to rehybridization of the sp^2 C-C bond and can result in adsorption behavior that is different from graphene.

In this work, the adsorption of 12 different metal adatoms on graphene is studied using first-principles density-functional theory (DFT). Details of our method are described in Sec. II. The adatoms chosen are often used in experiments and span a range of valences, including *s* and *p* valence metals, transition metals, and noble metals. The adsorption energy, geometry, density of states (DOS), dipole moment, work function, and magnetic moment are calculated. To augment previous work for alkalis on graphite[13] and other surfaces,[15,16] the issue of charge transfer is discussed, and for a subset of adatoms, charge transfer is determined quantitatively using two methods, one based on the density of states and the other based on the real-space-charge density. The large set of data resulting from this work is obtained with a uniform set of approximations, allowing for the direct comparison of values across the range of adatoms and the derivation of general adsorption trends.

Our results, described in Sec. III, show that many adatoms bind to graphene with an adsorption energy of ~1 eV. From the density of states, we determine that the adatoms considered in this work from groups I–III of the Periodic Table bond ionically to graphene, transferring close to one electron to graphene without significantly modifying the graphene

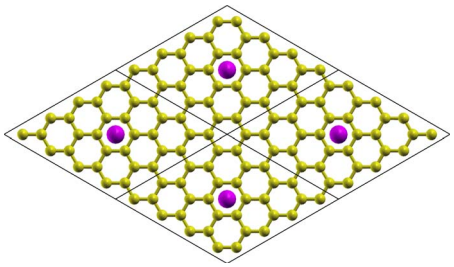

FIG. 1. (Color online) Adatom on the hollow site in a periodic 4×4 arrangement on a graphene surface.

electronic states; other transition, noble, and group IV metal adatoms modify the graphene states to a large degree, indicative of covalent bonding. Several adatoms induce a large dipole moment and work-function shift relative to isolated graphene. We find a strong relation between the work-function shift and the ionization potential (IP) of the isolated atom.

II. METHODS

Our calculations are performed within first-principles DFT under the generalized gradient approximation (GGA) of Perdew, Burke, and Ernzerhof (PBE),[17] including spin polarization. The Vienna Ab-initio Simulation Package (VASP) is used to perform all calculations.[18–20] Ion cores are modeled with projector augmented wave (PAW) potentials.[21,22] The semicore 1*s* states of Li, 2*p* states of Na, 3*p* states of K and Ca, and *d* states of Ga, In, Sn, Pd, and Au are treated explicitly as valence. A plane-wave basis set with a maximum plane-wave energy of 500 eV is used for the valence electron wave functions. All parameters in the calculation are chosen to converge the total energy to 0.01 eV.

Graphene has two C atoms arranged in a two-dimensional honeycomb lattice with a hexagonal primitive unit cell. We use our calculated graphene lattice constant of 2.47 Å, which is slightly larger than the experimental value of 2.46 Å. For notation, we let the *x* and *y* directions be parallel and the *z* direction perpendicular to the graphene plane.

The adatom-graphene system is modeled using one metal adatom in a 4×4 hexagonal graphene supercell (Fig. 1; we refer to the metal adatom arrangement as a 4×4 layer). This setup corresponds to a coverage of 1 adatom per 32 C atoms. The in-plane lattice constant is 9.88 Å, which is also the distance between neighboring adatoms. We use a supercell length of 15 Å in the *z* direction.

The calculation using the 4×4 coverage approximates the interaction of an isolated adatom with graphene. Although the adatom-adatom interaction is not negligible, the distance between adatoms is large enough that the overlap of the electronic states of neighboring adatoms is small. For K, the total energy of a 4×4 metal layer of K in the absence of graphene differs from that of the isolated K atom (described below) by less than 0.01 eV. Potassium has the largest atomic radius of all adatoms considered (2.20 Å; Ref. 23).

The adatom-graphene system lacks inversion symmetry and therefore has a net electric-dipole moment perpendicular to the surface. To remove spurious dipole interactions between periodic images along the *z* direction, we self-consistently apply corrections to the local electrostatic potential and the total energy.[24,25] These corrections are necessary in order to get the correct vacuum energy level, which we use to determine the work function. We find corrections to the total energy to be as large a 0.2 eV.

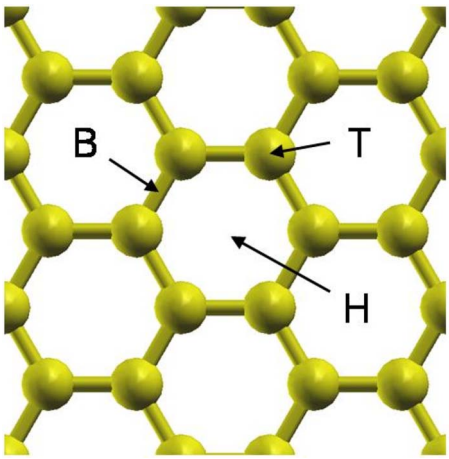

FIG. 2. (Color online) The three adsorption sites considered: hollow (*H*), bridge (*B*), and top (*T*).

Calculations for the isolated 4×4 graphene, isolated 4×4 adatom layer, and 4×4 adatom-graphene system are performed with the same-sized hexagonal supercell. The Brillouin zone is sampled with a $9\times9\times1$ Γ-centered *k*-point grid, and Gaussian smearing with a width of $\sigma=0.05$ eV is used for the occupation of the electronic levels. We consider the binding of the adatom on three sites of high symmetry: the hollow (*H*) site at the center of a hexagon, the bridge (*B*) site at the midpoint of a carbon-carbon bond, and the top (*T*) site directly above a carbon atom (Fig. 2). For each adsorption site for the adatom-graphene system, the adatom is relaxed along the *z* direction and the C ions in graphene in all directions until forces on the ions are less than 0.05 eV/Å. The supercell dimensions are kept fixed for all calculations.

To calculate adsorption energies, we also require the total energy of an isolated atom, which is approximated by the calculation with a single atom in a cubic supercell of length 14 Å. Only the Γ point of the Brillouin zone is sampled in this case.

III. RESULTS

A. Adsorption energy and geometry

In this work, we define the adsorption energy as

$$\Delta E = E_{\mathrm{ag}} - E_{\mathrm{a}} - E_{\mathrm{g}}, \tag{1}$$

where E_{ag} is the total energy per adatom of the 4×4 adatom layer on graphene, E_{a} is the total energy of an isolated atom, and E_{g} is the total energy of the isolated graphene per 4×4 supercell (containing 32 C atoms).

The adsorption geometry is obtained from the positions of the atoms after relaxation. The adatom height (*h*) is defined as the difference in *z* coordinate of the adatom and the aver-

age of the z coordinates of the C atoms in the graphene layer. The distance (d_{AC}) between the adatom and its nearest carbon atom(s) is also calculated. In some cases, the distortion of the graphene layer is significant. We quantify the distortion by computing the maximum deviation in the z direction of the C atoms in the graphene layer from the average of their positions.

Of the three adsorption sites considered, the site with the largest adsorption energy (minimum total energy) is referred to as the favored site. We assume that the most likely diffusion pathway between favored sites is via the high-symmetry site with the next largest adsorption energy. The energy difference between these two sites is referred to as the diffusion barrier (E_{diff}). More accurate determination of the diffusion barrier would require calculating the complete potential-energy surface or using, for example, the nudged elastic band method.[26] For all atoms which bind to the H or T sites (B site), the next largest adsorption energy is for the B site (T site).

Adsorption energies and structural properties for the three sites considered are summarized in Table I. Metal adatoms from groups I–III all bind most strongly to the H site. Within group III, the adsorption energy decreases monotonically with increasing atomic number; however, this trend is not followed by the alkali metals. Our calculated adsorption site, adsorption energies, and heights are in reasonably good quantitative agreement with previous calculations for alkalis[28–31] and for In.[32] There is not complete agreement on the nature of the bonding of Al with graphite among previous experimental and theoretical works,[33–37] but within our calculation, Al fits into the consistent picture that we find across the different elements.

For the alkalis, the relatively high ratios of adsorption energy to bulk cohesive energy suggest that alkalis are able to form 2D layers on the surface of graphene, as opposed to three-dimensional (3D) clusters, in agreement with experiments observing 2D alkali layer formation on graphite.[13] On the other hand, the ratio $\Delta E/E_c$ for group III elements is lower than for the alkalis, which is reasonable given the experimentally observed island or 3D cluster formation for Al and In on nanotubes or graphite.[9,10,33,34]

The general consensus from both experiment and theory is that for dispersed alkali adatoms, the bonding to graphite is mainly ionic.[13] In Sec. III B, we provide evidence that groups I–III adatoms bond ionically to graphene. Our result indicating that these elements adsorb to the H site is consistent with previous work for alkalis on metal surfaces[16] which shows that for ionic bonding, sites of high coordination are favored.

For each element from groups I–III, the adsorption energy and height for the B site are similar to the energy and height for the T site, while for the H site the adsorption energy is larger and the height is smaller. For an ionically bonded adatom, the equilibrium height results from a balance of the electrostatic attraction between oppositely charged adatom and surface and the short-range electron repulsion. Since the graphene electron density is lower at the H site than at the B or T sites, the adatom is stabilized closer to the surface. Thus ionic bonding appears to favor adsorption to the H site because, in addition to having a higher coordination as mentioned above, the adatom is also closer to the sheet, reducing the electrostatic energy (see also Ref. 38).

The diffusion barriers via the B site for adatoms from groups I–III are around 0.1 eV, with the exception of Li, which has a significantly smaller size than the other atoms. Within group I or group III, the trends in adsorption height or diffusion barrier are well correlated with atomic radius. For ionic bonding, as the adatom radius increases, its height increases, and the effect of the corrugation of the graphene is reduced. Elements from groups I–III do not distort the graphene sheet by a significant amount, even on the B or T sites, where the distortion is greatest. Thus the C-C bonds near the adatom retain their sp^2 character and do not rehybridize significantly with any adatom orbitals. This result provides further support for the ionic bonding picture.

The $3d$ transition-metal Ti has the largest adsorption energy of the adatoms considered, while Fe has a more modest adsorption energy. Like elements from groups I–III, Ti and Fe favor the H site. However, the diffusion barriers are much larger than those for groups I–III (about 0.5 eV). In addition, the H site-adsorption height for Fe is small compared with the other adatoms studied. As will be discussed in Sec. III B, Ti and Fe bond covalently with graphene. Covalent bonds are directional, and the bond formation depends on the adatom coordination. Therefore it is reasonable that the adsorption energy is strongly dependent on the adsorption site. Our calculations for binding energy and geometry are in reasonable agreement with previous calculations for Ti and Fe on graphene.[39–41] In contrast to the strong binding we observe in our calculations, some experiments suggest that the Ti-graphene interaction is weak.[42] This difference may be due to a larger Ti surface density in experiment than in our calculations, which may reduce the Ti-surface interaction.

Though Pd has a filled d shell, it binds strongly to the B site of graphene, implying covalent bonding. The electronic structure presented in Sec. III B shows that like Ti and Fe, Pd adsorption involves hybridization of adatom d orbitals with the orbitals of graphene. However, the observation of d orbital hybridization alone is not enough to determine the favored adsorption site for a given adatom.

Although, like the alkalis, the Au atom has a single s valence electron, the Au adsorption energy is small. Sn adsorption is slightly stronger but is also weak relative to other adatoms. Adsorption of these elements to graphene likely involves van der Waals forces, which are not captured by DFT with the GGA. To the extent that our calculations accurately describe Au and Sn adsorption on graphene, the bonding is covalent; such bonding is consistent with adsorption to the T site, which allows for greater direct hybridization between the C atom and the adatom than adsorption to the H site.

In contrast to group I–III elements, Pd, Au, and Sn adatoms all induce noticeable distortion ($\geq$0.07 Å) of the graphene sheet upon adsorption. The strong distortion likely changes some of the graphene sp^2-like orbital character to a more covalently reactive sp^3-like character. These three adatoms can diffuse readily along the hexagonal C bond network. For Au and Sn, the diffusion barrier is very small

TABLE I. Energetic and structural properties for the hollow (H), bridge (B), and top (T) sites for the 12 adatoms considered in this work. The properties listed are the binding energy (ΔE), difference between binding energy and binding energy of lowest energy site ($E_a^{\max}-\Delta E$), adatom height (h), adatom-carbon distance (d_{AC}), and graphene distortion (d_{GC}). For reference, we include the experimental cohesive energy per atom of the bulk metal (E_c) from Ref. 27 and the ratio of the adsorption energy to the bulk cohesive energy ($\Delta E/E_c$).

Atom	Site	ΔE (eV)	E_c (eV)	$\Delta E/E_c$	$E_a^{\max}-\Delta E$ (eV)	h (Å)	d_{AC} (Å)	d_{GC} (10^{-1} Å)
	H	1.096	1.630	0.672		1.71	2.23	0.0
Li	B	0.773			0.322	1.88	2.09	0.2
	T	0.754			0.342	1.89	2.02	0.3
	H	0.462	1.113	0.415		2.28	2.70	0.1
Na	B	0.393			0.069	2.44	2.59	0.1
	T	0.389			0.074	2.49	2.54	0.1
	H	0.802	0.934	0.859		2.60	2.99	0.1
K	B	0.739			0.063	2.67	2.85	0.3
	T	0.733			0.069	2.67	2.77	0.2
	H	0.632	1.840	0.343		2.29	2.72	0.1
Ca	B	0.484			0.148	2.33	2.53	0.2
	T	0.478			0.154	2.34	2.46	0.2
	H	1.042	3.390	0.307		2.13	2.56	0.1
Al	B	0.927			0.115	2.22	2.33	0.1
	T	0.911			0.131	2.22	2.24	0.2
	H	0.858	2.810	0.305		2.20	2.63	0.0
Ga	B	0.762			0.096	2.30	2.41	0.0
	T	0.749			0.109	2.31	2.33	0.1
	H	0.690	2.520	0.274		2.45	2.83	0.1
In	B	0.622			0.069	2.53	2.63	0.0
	T	0.614			0.077	2.55	2.56	0.1
	H	0.114			0.142	3.19	3.48	0.1
Sn	B	0.253			0.003	2.79	2.81	0.8
	T	0.256	3.140	0.082		2.82	2.75	0.7
	H	1.869	4.850	0.385		1.80	2.33	0.2
Ti	B	1.301			0.568	2.05	2.27	0.3
	T	1.301			0.568	2.00	2.18	0.3
	H	0.748	4.280	0.175		1.53	2.11	0.1
Fe	B	0.231			0.517	2.22	2.35	0.0
	T	0.149			0.599	2.18	2.13	0.5
	H	0.852			0.230	2.03	2.46	0.3
Pd	B	1.081	3.890	0.278		2.21	2.18	1.4
	T	1.044			0.038	2.21	2.10	1.1
	H	0.085			0.011	3.53	3.80	0.0
Au	B	0.089			0.007	3.06	3.11	0.4
	T	0.096	3.810	0.025		2.69	2.55	1.4

(<0.01 eV), and since the adsorption energies are small, the adsorption heights are correspondingly large. Our results for Au are in good agreement with previous calculations using the GGA (Refs. 32, 43, and 44); previous calculations with the local-density approximation (LDA) give somewhat larger adsorption energies.[32,45]

B. Electronic structure

In this section, we compute the electronic structure of the adatom-graphene system and identify general trends across the different adatoms considered. The Kohn-Sham DOS is computed for each adatom on the favored adsorption site using a $24\times24\times1$ Γ-centered Brillouin-zone sampling, and

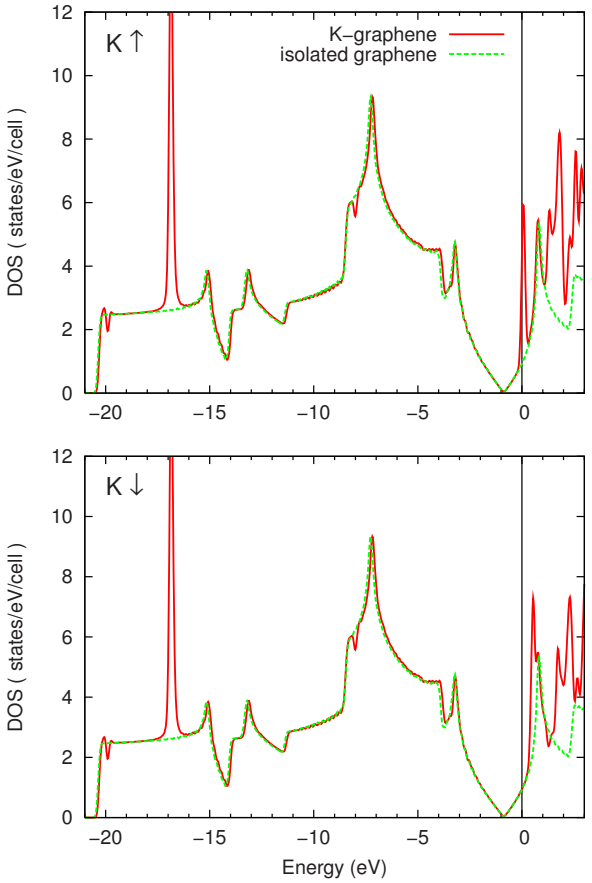

FIG. 3. (Color online) Spin-up (top) and spin-down (bottom) total DOS for K on the H site of graphene and for isolated graphene. The energy is relative to E_F of the K-graphene system. The curves are aligned at the Dirac point.

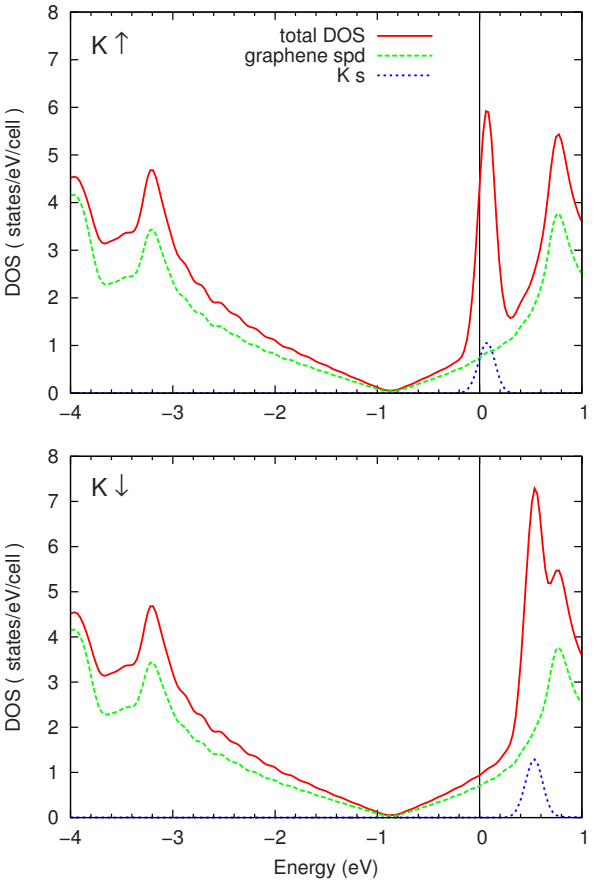

FIG. 4. (Color online) Spin-up (top) and spin-down (bottom) total DOS, PDOS on the graphene states, and PDOS on the K s states for K on the H site of graphene. The energy is relative to E_F.

the energy eigenvalues are smeared with Gaussians of width σ=0.1 eV. To generate the projected density of states (PDOS), the electron wave functions are projected onto spherical harmonics localized within a sphere centered about each atom. For the C atoms in graphene, the sphere radius is chosen to be 1.03 Å. For each adatom, the sphere radius is chosen to be the atomic radius, taken from Ref. 23.

We first consider alkali adsorption using K as an example. Of the metal adsorbates considered here, the alkalis are closest to ideal ionic bonding. Figure 3 shows the DOS for K on the graphene H site and the DOS for isolated graphene, for both spin up and spin down. For each curve, the Dirac point of the graphene (where the DOS is zero) is clearly visible. In the plots, we shift the isolated graphene DOS to align its Dirac point with that of the K-graphene DOS. We denote the energy of the Dirac point by E_D. Near and below the Fermi level (E_F), the isolated graphene DOS closely matches that of the adatom-graphene system, except near clearly defined peaks at −17 eV and just above E_F (corresponding to 3p and 4s adatom states, respectively), showing that the graphene states are nearly unaltered by the adsorption of K adatoms.

Figure 4 shows the same K-graphene DOS near the E_F along with the projection of the DOS onto graphene and the K s state. The spin-up 4s peak lies close to the Fermi level and is partially occupied, while the spin-down 4s peak lies approximately 0.5 eV above E_F and is unoccupied. The positions of these peaks above E_F are probably underestimated, since it is well known that GGA Kohn-Sham energy eigenvalues often differ from the true quasiparticle energies. There is no evidence for hybridization between the K 4s peaks and the graphene states; the PDOS of the graphene shows no peaks near the K 4s levels. Furthermore, the broadening of the K 4s peaks due to interaction with the graphene is small.

For K on graphene, the Fermi level is shifted higher in energy relative to E_D, reflecting a greater occupation of graphene states. Also, in an isolated atom, the spin-up 4s peak is fully occupied, while in the adatom-graphene system the spin-up 4s peak is only partially occupied. These observations suggest that the bonding is predominantly ionic and that close to one electron of charge (e) is transferred from the 4s state of the adatom to the graphene states.

Similar characteristics for the DOS are found for Na, including splitting of the 3s valence spin-up and spin-down peaks, with partial occupation of the 3s spin-up peak and an increase in E_F relative to E_D. For Li, the 2s spin-up and spin-down states are degenerate and lie about 0.9 eV above E_F, suggesting that more charge is transferred to graphene by Li than by Na or K. The degeneracy of the Li spin-up and spin-down 2s states and the splitting and partial occupancy of the Na 3s and K 4s states are in good agreement with previous theoretical calculations.[28,29] The ionic bonding pic-

TABLE II. Electronic properties for the favored adsorption site for the 12 adatoms considered in this work. The properties listed are the electric-dipole moment per adatom (p), work function (Φ), magnetic moment per adatom of the adatom-graphene system (μ_{AG}), and magnetic moment of the isolated atom (μ_A). The calculated work function for isolated graphene is 4.26 eV. Also included is the experimental ionization potential (IP) of the isolated atom from Ref. 46. The electric-dipole moments are in units of debye (D), and the magnetic moments are given in Bohr magnetons (μ_B).

Atom	Site	p (D)	Φ (eV)	μ_{AG} (μ_B)	μ_A (μ_B)	IP (eV)
Li	H	3.46	2.72	0.00	1.00	5.39
Na	H	2.90	2.21	0.27	1.00	5.14
K	H	4.48	1.49	0.17	1.00	4.34
Ca	H	0.85	3.18	1.04	0.00	6.11
Al	H	0.93	3.08	0.00	1.00	5.99
Ga	H	1.83	2.66	0.00	1.00	6.00
In	H	2.57	2.34	0.00	1.00	5.79
Sn	T	0.19	3.81	1.81	2.00	7.34
Ti	H	1.39	3.16	3.41	4.00	6.83
Fe	H	1.84	3.24	2.03	4.00	7.90
Pd	B	1.23	3.61	0.00	0.00	8.34
Au	T	−1.29	4.88	0.96	1.00	9.23

ture for the alkalis from the DOS agrees with our calculated energetic and structural properties and with the consensus from previous experiment and theory.[13]

The adsorption of Na or K adatoms on graphene leads to a net magnetic moment (Table II) that is reduced from that of the isolated atom. This reduction results from partial charge transfer to the graphene, whose states are not spin polarized in the case of ionic bonding. One should exercise care in interpreting the magnetic-moment results, which may be sensitive to adatom arrangement. The 4×4 adatom structure used for these calculations has not been observed experimentally; in addition, the GGA may not accurately describe the occupation of such localized adatom states.

In the case of Ca, the isolated atom has a filled $4s$ shell with two electrons. However, when Ca is adsorbed onto the graphene H site, its spin-down $4s$ peak lies above E_F and is unoccupied, resulting in a magnetic moment of about $1\mu_B$/adatom. Experiments assessing the possibility of such a strong localized moment would be of interest. As with K, little hybridization of the $4s$ states with the graphene sheet is observed.

We now discuss the PDOS for Al on the H site (Fig. 5), which is respresentative of the group III elements. These elements have two s valence electrons and one p valence electron in the outermost shell. Compared with the alkalis and Ca, Al adsorption affects the graphene electronic structure to a greater degree. The $3s$ state of Al appears to split and hybridize with the graphene states at −8.6 and −3.3 eV relative to E_F. The Al $3p$ peak lies 1.3 eV above E_F and is noticeably broadened due to the Al-graphene interaction. Nevertheless, the Dirac point is still clearly visible. Between E_D and E_F, the states are mostly from the graphene, and the

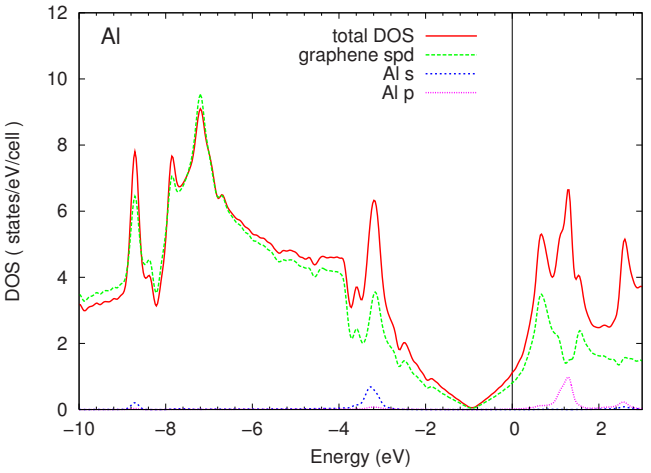

FIG. 5. (Color online) Spin-up total DOS, PDOS on the graphene states, and PDOS on the Al s and p states for Al on the H site of graphene. Spin-up and spin-down states are degenerate. The energy is relative to E_F.

DOS appears to be minimally altered from the isolated graphene case. Therefore, as for the alkalis, it is reasonable to characterize the bonding as ionic, involving charge transfer of nearly one electron per adatom to graphene. Although the interaction of the Al $3s$ state with graphene may contribute somewhat to the overall bonding, it may not be important for properties which depend mostly upon the states at E_F, such as transport.

For Al, Ga, and In, the valence p peak remains above E_F, so that in all cases, close to one electron per adatom is transferred to graphene. Since there is little occupation of the valence p peak, the up- and down-spin states are degenerate, and there is no net magnetic moment for the group III elements. Other features of the PDOS mentioned for Al are qualitatively the same for Ga and In. The ionic characteristics of the PDOS for group III elements are consistent with the energetic and structural information discussed in Sec. III A. For In, the position of the $5p$ peak and the large charge transfer inferred from the PDOS are in good agreement with previous *ab initio* calculations.[32]

Unlike the elements from groups I–III, the transition metals Ti, Fe, and Pd significantly alter the graphene electronic structure. An important common feature in the DOS for these adatoms on graphene is the strong hybridization of the adatom d states with the graphene states to form covalent bonds. The PDOS for Ti on the H site of graphene is shown in Fig. 6. Strong hybridization of Ti $3d$ states and graphene states is evident from the prominent peaks in the PDOS. In the spin-up PDOS, these hybrid Ti $3d$/graphene states lie in a broad range about E_F. Because the graphene states are strongly altered, the Dirac point is no longer evident. In the spin-down PDOS, the Ti $3d$ states lie mostly above E_F. In this case, it appears that E_D lies below E_F, and one might infer electron transfer from Ti to graphene, though for covalent bonding, the concept of charge transfer is more ambiguous than for ionic bonding. Charge transfer helps us to explain the reduction in magnetic moment from the isolated to the adsorbed atom (Table II). Electrons which are spin polarized in the isolated atom are transferred to less polarized

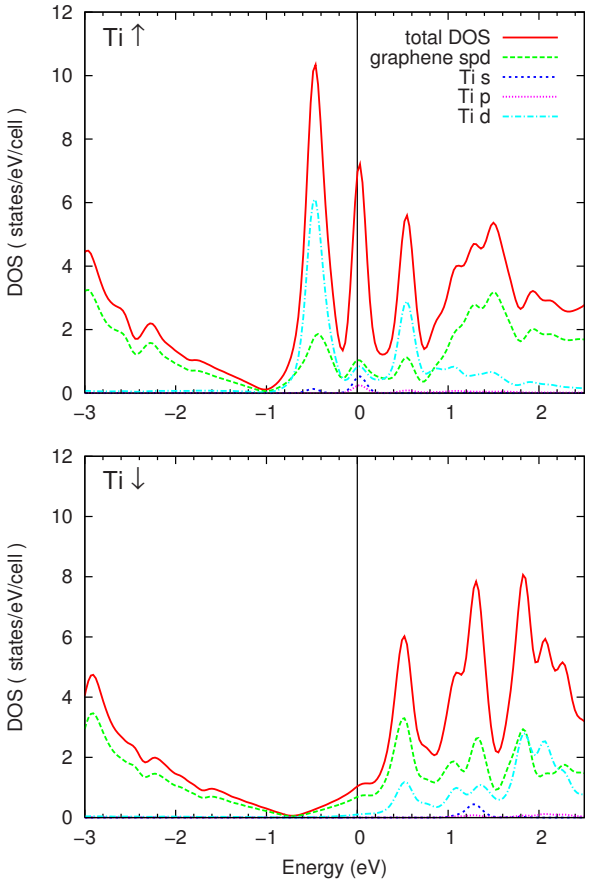

FIG. 6. (Color online) Spin-up (top) and spin-down (bottom) total DOS, PDOS on the graphene states, and PDOS on the Ti s, p, and d states for Ti on the H site of graphene. The energy is relative to E_F.

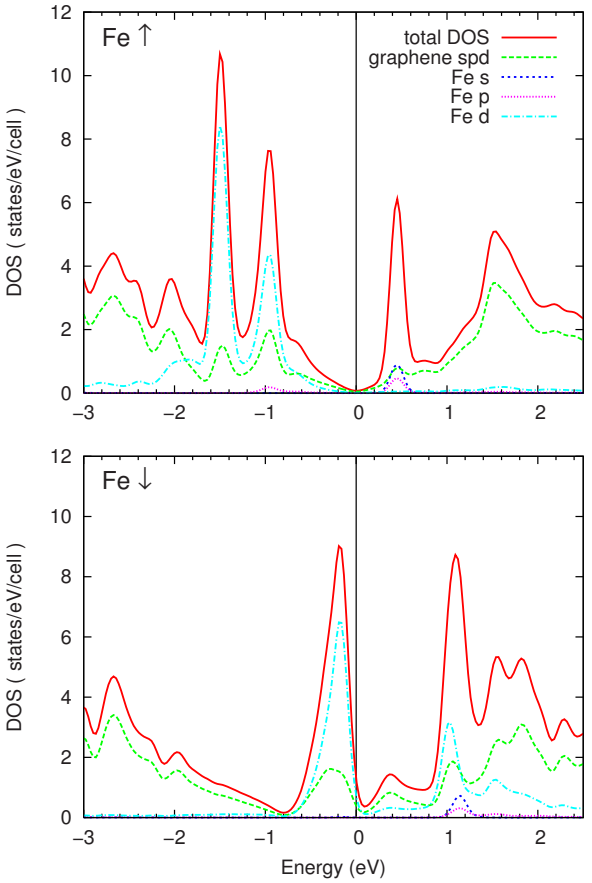

FIG. 7. (Color online) Spin-up (top) and spin-down (bottom) total DOS, PDOS on the graphene states, and PDOS on the Fe s, p, and d states for Fe on the H site of graphene. The energy is relative to E_F.

graphene states when the atom is adsorbed on graphene.[47] The hybridization, charge transfer, and magnetic moment are in reasonable agreement with previous calculations.[39]

As for Ti, the PDOS for Fe on the H site (Fig. 7) shows that there is covalent bonding and hybridization between 3d states and graphene states. The spin-up 3d states of Fe are occupied and are split into two main peaks plus a broad band spanning several eV. The spin-down 3d states of Fe also consist of two main peaks, one at E_F, as well as broad features. The spin-up and spin-down 4s states lie approximately 0.4 and 1.1 eV above E_F. The DOS illustrates that approximately two electrons are shifted from the 4s states in atomic Fe to the spin-down 3d states in the Fe-graphene system. Consequently, the magnetic moment is reduced from $4\mu_B$ for the isolated Fe atom to $2.03\mu_B$/adatom for Fe adsorbed on graphene. The hybridization of the spin-down 3d states lowers their energy relative to the 4s states, explaining this transfer of electrons.

Since the graphene states are altered by Fe adsorption, the Dirac point can no longer be clearly identified. The DOS suggests that E_F does not shift much from E_D, indicating that little, if any, charge is transferred between the adatom and graphene. However, as for Ti, the applicability of the charge-transfer concept is unclear.

Interestingly, although the Pd atom has a filled 4d shell, the 4d orbitals strongly hybridize with the graphene states when Pd is adsorbed on the B site (Fig. 8). These states lie below E_F, and there is no magnetic moment. The Pd 5s peak lies about 0.9 eV above E_F, and the Fermi level of graphene appears to remain at the Dirac point. In Pd and Fe, the bond-

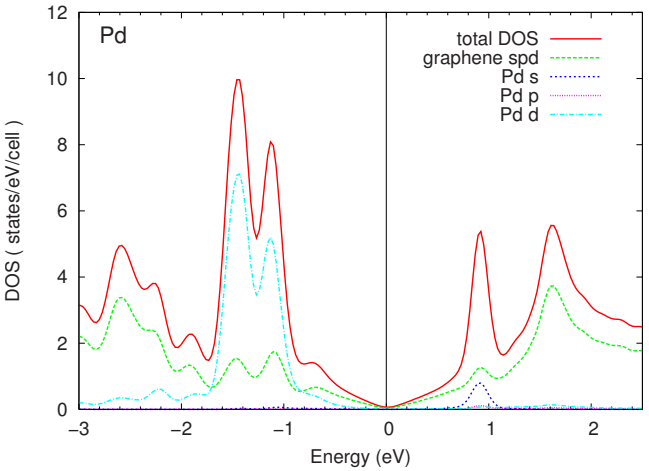

FIG. 8. (Color online) Spin up total DOS, PDOS on the graphene states, and PDOS on the Pd s, p, and d states for Pd on the B site of graphene. Spin-up and spin-down states are degenerate. The energy is relative to E_F.

ing is almost completely covalent. For Au and Sn, near E_F, the $6s$ and $5p$ orbitals, respectively, hybridize with the graphene states. However, as noted above, the GGA may not be an accurate approximation for the bonding of these two elements to graphene.

C. Charge transfer

For adatoms from groups I–III, the DOS provides evidence for ionic bonding and charge transfer between the adsorbate and substrate. Extracting a quantitative value for charge transfer from *ab initio* calculations is useful for comparing with both experiment and simple models. However, charge transfer is an ambiguous quantity and there is no unique definition. Some discussion of the concept of charge transfer in the context of adsorption to metal surfaces can be found in Ref. 15. Charge transfer is most sensible in the context of ionic bonding. In the case of covalent bonding, charge is shared in the bond between adsorbate and substrate, and thus the charge-transfer concept is less relevant.

For alkalis on graphite, various definitions of charge transfer are considered in several previous works.[28,30,48–50] In this work, we compare two definitions of charge transfer. One is based on the shift in E_F relative to the graphene DOS resulting from adatom adsorption. The other is based on integration of the charge density in real space. We apply these definitions to groups I–III adatoms. The other adatoms considered in this work bond with some degree of covalency to graphene and do not permit the same analysis.

1. Charge transfer from the DOS

The DOS of the adatom-graphene system can be used to determine the charge transfer, assuming that the graphene states remain unchanged due to adatom adsorption (aside from a rigid shift). As discussed in Sec. III B, this assumption is good for the alkalis and is reasonable for groups II and III as well. For these systems, electrons are donated to the graphene, filling the rigid graphene states and thereby shifting the Fermi level up from the Dirac point. To calculate charge transfer from the adatom-graphene DOS, the Dirac point is identified, and the shift in Fermi level

$$\Delta E_F = E_F - E_D \tag{2}$$

is determined. The charge transfer Δq_{DOS} is given by the integral of the isolated graphene DOS from E_D to $E_D+\Delta E_F$. The Fermi-level shift ΔE_F and charge transfer Δq_{DOS} are given in Table III for each of the elements in groups I–III considered in this work. A positive charge transfer indicates transfer of electrons from the adatom to graphene.

It is interesting that $\Delta E_F \approx 0.9$ eV for all groups I–III elements we considered (although a small difference in ΔE_F can give a significant difference in Δq_{DOS}). The largest charge transfer is for Li, but Na, K, and Ca all transfer less charge than the group III elements.

Similar methods have been used previously to estimate charge transfer for K on graphite at a low coverage using Fermi-level shifts determined from experiments. Charge transfer has been estimated to be around $0.7e$ from electron energy-loss spectroscopy[51] at a coverage of less than 0.1 monolayer (ML). For K, a coverage of 1 ML corresponds to a 2×2 hexagonal adsorbate structure. This value is in reasonable agreement with our results, although our coverage is at least 2.5 times greater than that in experiment. Using a Fermi-level shift determined from photoemission, the charge transfer has been estimated to be around $0.1e$,[52,53] significantly less than our and most other previous results for charge transfer.[13] Issues related to adatom coverage are discussed further in Sec. III D.

TABLE III. Fermi level shift relative to the graphene states (ΔE_F), charge transfer determined from the DOS (Δq_{DOS}), adsorbate-substrate cutoff distance (R_{cut}), and charge transfer from charge-density integration (Δq_ρ) for adatoms from groups I–III.

Atom	ΔE_F (eV)	Δq_{DOS} (e)	R_{cut} (Å)	Δq_ρ (e)
Li	0.95	0.90	1.64	0.39
Na	0.86	0.73	1.57	0.32
K	0.88	0.76	1.64	0.41
Ca	0.89	0.78	1.44	0.18
Al	0.94	0.88	1.37	0.14
Ga	0.94	0.88	1.44	0.21
In	0.92	0.84	1.51	0.27

2. Charge transfer from the charge density

Partitioning the charge density in real space can be used to define charge transfer as well. (In what follows, the charge density refers to the valence electron charge density.) First, we define the charge-density difference as

$$\Delta\rho(\mathbf{r}) = \rho_{\mathrm{ag}}(\mathbf{r}) - \rho_{\mathrm{a}}^{\mathrm{layer}}(\mathbf{r}) - \rho_{\mathrm{g}}^{\mathrm{relaxed}}(\mathbf{r}). \tag{3}$$

For all quantities in Eq. (3), the charge density is computed in the same hexagonal supercell. The quantity ρ_{ag} is the charge density of the adatom-graphene system. The charge density of the 4×4 adatom layer without graphene, $\rho_{\mathrm{a}}^{\mathrm{layer}}$, is calculated with the adatom in the same position in the supercell as for the adatom-graphene calculation. The quantity $\rho_{\mathrm{g}}^{\mathrm{relaxed}}$ is the charge density of an isolated 4×4 graphene layer, computed with the atoms fixed to their relaxed coordinates from the adatom-graphene calculations; these coordinates differ from those of isolated graphene. The charge-density difference quantifies the redistribution of electron charge due to the adatom-graphene interaction.

As an example, Fig. 9 shows the x-y planar-averaged charge-density difference ($\Delta\rho_{\mathrm{av}}$) as a function of z for K on the H site. The position of the graphene sheet at $z=0$ Å and the position of the adatom at $z=2.60$ Å are indicated by vertical lines. The plot illustrates electron transfer from the adatom to the graphene with a large overall electron density increase near the graphene sheet and an electron density decrease near the adatom.

To determine the charge transfer using the spatial charge density, the regions of space belonging to the graphene or the adatom must be specified, introducing a degree of arbitrariness to the definition. For the purpose of comparison, we

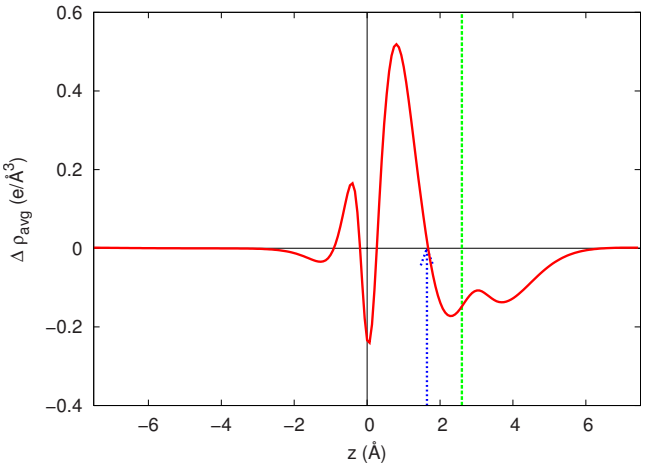

FIG. 9. (Color online) The x-y planar-averaged electron charge-density difference ($\Delta\rho_{\mathrm{av}}$) for K on graphene H site as a function of position in the z direction. Two vertical lines indicate the position of the graphene sheet (0 Å) and the position of the adatom (1.64 Å). The arrow at 1.64 Å indicates R_{cut} used in calculating Δq_ρ.

adopt the definition used in several previous works.[28,30,48–50] An adsorbate-substrate cutoff distance R_{cut} is defined as the distance from the graphene plane to the point between the plane and the adatom at which charge accumulation changes to charge depletion for electron transfer from the adatom to the graphene (or vice versa for opposite electron transfer). For example, in Fig. 9, the region with $z<R_{\mathrm{cut}}$ is assigned to the substrate, and the region with $z>R_{\mathrm{cut}}$ is assigned to the adatom. The charge transfer Δq_ρ is given by the integral of the charge-density difference in the substrate region. The results for R_{cut} and Δq_ρ are given in Table III for adatoms from groups I–III.

For the alkalis, R_{cut}, Δq_ρ, and plots of the planar-averaged charge-density difference are consistent with previous calculations,[30] with small differences likely coming from the different numbers of graphene layers used. Within group I or group III, the values for R_{cut} and Δq_ρ are similar. The alkalis have greater charge transfer than the other elements. For group III, R_{cut} and Δq_ρ increase monotonically with atomic number. The cutoff distance R_{cut} is nearly the same for all the alkalis (as noted in Ref. 30) but is different from R_{cut} for the group III elements. That the effective "thickness" of the graphene depends on the adsorbate is an indication of the arbitrariness of the charge-transfer definition.

3. Comparison of charge-transfer definitions

The charge-transfer values differ significantly depending on the definition, with $\Delta q_{\mathrm{DOS}}>\Delta q_\rho$ for a given element. Also, Δq_{DOS} is larger for the group III elements than for the alkalis (aside from Li), while the reverse is true for Δq_ρ. It is not surprising that the two definitions give different values, since the charge density associated with an electronic state with a defined energy can be spatially extended. Both definitions have reasonably simple pictures. The one that is more meaningful depends on the physical properties of interest. Examining the DOS would be more useful if one was interested in the carrier concentration of graphene, while the charge-density definition might be more suited for simple electrostatic models of the adatom-graphene interaction or for interpreting core-level shift measurements.

D. Dipole moment and work function

The electric-dipole moment perpendicular to the graphene sheet is an alternative to charge transfer for quantitatively describing the real-space-charge rearrangement due to adatom-graphene interaction. For ionically bonded adatoms, the dipole moment has a large contribution from charge transfer between adatom and substrate, but rearrangement of charge in covalent bonds and polarization of semicore states localized on the adatom also play a role. These contributions could also apply to covalently bonded adatoms.

Unlike charge transfer, the dipole moment is well defined for both ionic and covalent cases considered here. We compute the dipole moment p in the z direction for the unit cell of the adatom-graphene system as

$$p=-\int \rho(z)z\,dz+\sum_i Z_i e z_i, \tag{4}$$

where $\rho(z)$ is the valence electron density integrated over the x-y plane [$\rho(z)\geq 0$ by definition], i indexes the ion, Z_i is the net atomic number of ion i, e is the electronic charge ($e>0$), and z_i is the z coordinate of ion i. The sum and integral are over the unit cell. Since there is one adatom per unit cell, p gives the dipole moment per adatom.

In general, adatom adsorption on graphene is expected to alter the Fermi level and dipole moment of the system, and there can be a large change in work function relative to isolated graphene. We define the work function as

$$\Phi=E_{\mathrm{vac}}-E_F, \tag{5}$$

where E_{vac} is the reference vacuum energy. In our calculation, E_{vac} is determined from the electrostatic potential in the vacuum region, far enough away from the adatom-graphene system in the z direction that the value is converged. Because the adsorption is only one side of the graphene sheet, the vacuum energies on the two sides of the graphene sheet differ, with the potential difference proportional to the dipole moment (to leading order in multipoles) via

$$\Delta V=-4\pi e n_a p, \tag{6}$$

where n_a is the number of adatoms per unit area on the graphene surface ($n_a=1.18\times10^{14}$ adatoms/cm^2 for our 4×4 supercell). We use the term "dipole potential" to refer to this potential difference ΔV. In calculating the work function, E_{vac} is defined as the vacuum energy on the side of graphene that the adatoms are adsorbed to. The work function of isolated graphene is calculated to be 4.26 eV, an underestimate of the experimental value for graphite (about 4.6 eV) (Ref. 54) but consistent with other DFT calculations using the PBE functional.[55] This ~10% underestimation is not expected to qualitatively affect the broad trends described below.

The calculated dipole moment per adatom and work function for each adatom are listed in Table II. Of the adatoms

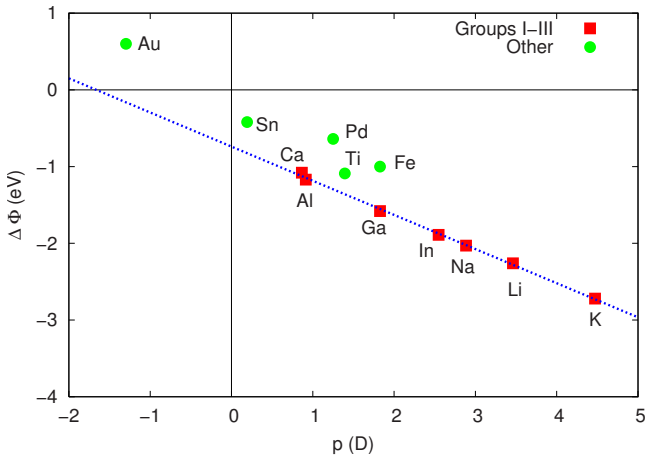

FIG. 10. (Color online) Plot of the work-function shift ($\Delta\Phi$) relative to isolated graphene versus dipole moment (p) for the 4 $\times$4 adatom coverage. The red squares are elements from groups I–III; other elements are marked by green circles. The dotted blue line is given by Eq. (7).

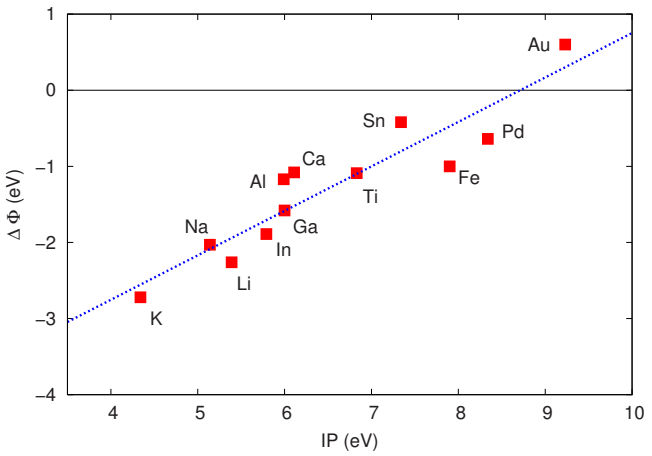

FIG. 11. (Color online) Plot of calculated work-function shift ($\Delta\Phi$) for the 4$\times$4 coverage versus IP from experiment (Ref. 46). The dotted line is given by Eq. (8).

considered, the alkalis generate the largest dipole moments and the largest decreases in work function. Other adatoms with ionic character (groups II and III) and even the covalently bonded adatoms also decrease the work function of graphene noticeably. In contrast, Au adatoms increase the work function of graphene.

Figure 10 shows a plot of the work-function shift ($\Delta\Phi$) relative to isolated graphene versus the dipole moment for the 4$\times$4 adatom arrangement considered here. Remarkably, the adatoms from groups I–III lie on a straight line given by the sum of the dipole potential [Eq. (6)] and an offset energy (E_{off}),

$$\Delta\Phi = -4\pi e n_a p - E_{\text{off}}. \tag{7}$$

Fitting this equation to the data for groups I–III gives E_{off} =0.74 eV. The observed linear relationship is consistent with the ionic bonding picture obtained from other data presented in this work. In particular, the fitted value for E_{off} is close to ΔE_F for these adatoms, which is about 0.9 eV (Table III). Equation (7) indicates that two dominant contributions to $\Delta\Phi$ for ionically bonded adatoms are: (i) the dipole potential, which shifts the graphene states rigidly with respect to the vacuum, and (ii) the filling of graphene states due to electron transfer from the adatom, resulting in a shift of the Fermi level relative to the graphene states.

For alkali adatoms on bulk metal surfaces, previous work has shown that to first approximation the work-function shift is simply given by the dipole potential, $\Delta\Phi = -4\pi e n_a p$.[56] For a bulk metal surface, any charge transfer between adatom and substrate changes E_F by an infinitesimal amount, so there is a negligible Fermi-level shift relative to the metal electronic states. On the other hand, since graphene is two dimensional and has a small DOS near E_F, charge transfer from adatom adsorption does result in a finite band filling term that contributes significantly to $\Delta\Phi$. Thus the ionic bonding picture for adsorption on graphene is consistent with that for adsorption on metals.

In Fig. 10, the data for adatoms not in groups I–III lie above the plotted line and are not collinear, possibly indicating that these adatoms each have different band filling terms that are smaller than 0.74 eV, which implies smaller charge transfer than for adatoms from groups I–III. It is also possible that, for these adatoms, $\Delta\Phi$ is not simply described as the sum of a dipole potential term and a band filling term. These observations are consistent with evidence from the binding energy, geometry, and DOS that their bonding is more covalent and less ionic in character.

Figure 11 shows that $\Delta\Phi$ is well correlated with the experimental IP of the isolated atom.[46] We fit the values of $\Delta\Phi$ and IP for the 12 species to a line and obtain the following relation for the 4$\times$4 coverage:

$$\Delta\Phi = 0.58\ \text{IP} - 5.09\ \text{eV}, \tag{8}$$

where $\Delta\Phi$ and IP are in units of eV. The overall trend of larger decreases in Φ for smaller IP values is reasonable, since Φ (IP) is the energy to remove an electron from the adatom-graphene system (isolated atom). Within the ionic picture of bonding, adatom species with lower IPs are more likely to transfer their outer-shell electrons to the graphene sheet, thereby both creating a larger dipole layer and raising E_F relative to vacuum to a greater degree. However, it is interesting to note that adatoms with covalent character also follow the general trend relating $\Delta\Phi$ and IP.

We now remark on the possible coverage dependence of our results. Decreasing the coverage would decrease n_a and E_{off} in Eq. (7), but we would not expect p to change significantly. Therefore we would expect the line in Fig. 10 to shift up and its slope to decrease in magnitude. Going to a high coverage would increase n_a but would also affect p and E_{off} due to increased adatom-adatom interaction, and a linear relation between $\Delta\Phi$ and p might no longer hold. In Fig. 11, we would also expect the slope to change monotonically with the coverage if adatom-adatom interactions are small, but the linear relation between $\Delta\Phi$ and the IP also might not hold at high coverages.

The adatom coverage (θ) and arrangement are important to consider when comparing our results to experiment. Previous experiments measuring $\Delta\Phi$ for adatoms on graphite focus mainly on K. Experimentally, K is observed to form a dispersed phase at low coverages on graphite, with a large adatom-adatom spacing. As the coverage is increased, the K-K spacing decreases until a critical coverage θ_c is reached. Above θ_c, hexagonal 2×2 K islands form, and the islands are separated by a dispersed phase with spacing corresponding to a 7×7 structure. Further increasing the coverage causes the islands to grow until a full 2×2 monolayer of K is formed (θ=1 ML for K).[57,58]

The 4×4 structure used in this work corresponds to a coverage θ=0.25 ML, which may be above the critical coverage ($\theta_c \approx 0.1-0.3$ ML; Refs. 57 and 59). Therefore, experimentally, the 0.25 ML coverage might consist of a mix of 2×2 islands and the dispersed phase, not a uniform 4×4 phase.

The work function for K on graphite as a function of coverage has been measured experimentally by the retarding potential method and by photoemission spectroscopy.[59] The work-function shift relative to clean graphite at θ=0.25 ML was measured to be about −1.6 eV, while our calculation for the 4×4 structure gives $\Delta\Phi=-2.77$ eV.

The discrepancies between our results and experiment are reasonable if we consider the differences between the 2×2 islands, the dispersed phase, and the 4×4 structure. The 2×2 island structure was experimentally reported to be metallic,[57] and compared with the dispersed phase there is less charge transfer and a smaller dipole moment per adatom. For the 2×2 structure, the work-function approaches the value for bulk metallic K.[59] At the hypothetical 4×4 structure, it is possible to obtain a large $\Delta\Phi$ because compared to the more dispersed phase, there is a higher density of polarized adatoms, and compared to the metallic 2×2 phase, there is greater polarization and a larger dipole potential contributing to the work-function shift.

IV. CONCLUSION

In this paper, the adsorption of 12 different metal adatoms on graphene is studied using first-principles density-functional theory. Calculations of adsorption energy, geometry, density of states, charge transfer, dipole moment, and work function give a consistent picture of bonding for the adatoms considered. Adatoms from groups I–III exhibit characteristics of ionic bonding, including adsorption to the *H* site, small distortion of the graphene sheet, little change in the graphene electronic states, and significant charge-transfer and work-function shifts. For these adatoms, charge transfer is calculated quantitatively using two methods, one based on the DOS and the other based on the integration of the real-space-charge density. The observed trends differ for these two definitions, demonstrating their different physical meanings. The work function can be understood to have two main contributions coming from the dipole potential and from the Fermi-level shift due to graphene band filling. Transition metal atoms with *d* valence electrons, noble metals, and group IV elements exhibit covalent bonding characteristics with strong hybridization of adatom and graphene electronic states. The utility of the charge-transfer concept is less clear than in the ionic case, but both ionic and covalent adatoms follow a linear relationship between $\Delta\Phi$ and the IP. Our work can serve as a basis for future experimental and theoretical studies of adsorption on graphene.

ACKNOWLEDGMENTS

This work was supported by National Science Foundation under Grant No. DMR07-05941. This work was also supported by the Director, Office of Science, Office of Basic Energy Sciences, U.S. Department of Energy under Contract No. DE-AC02-05CH11231. Portions of the work were performed at the Molecular Foundry, Lawrence Berkeley National Laboratory under Contract No. DE-AC02-05CH11231. Computational resources have been provided by NSF through TeraGrid resources at Indiana University, SDSC, and TACC and by DOE at the NERSC facility at Lawrence Berkeley National Laboratory. Figures 1 and 2 were generated using the XCRYSDEN program.[60]

[1] R. Saito, G. Dresselhaus, and M. S. Dresselhaus, *Physical Properties of Carbon Nanotubes* (Imperial College, London, 1998).
[2] A. K. Geim and K. S. Novoselov, Nat. Mater. **6**, 183 (2007).
[3] R. S. Lee, H. J. Kim, J. E. Fischer, A. Thess, and R. E. Smalley, Nature (London) **388**, 255 (1997).
[4] A. M. Rao, P. C. Eklund, S. Bandow, A. Thess, and R. E. Smalley, Nature (London) **388**, 257 (1997).
[5] M. Radosavljević, J. Appenzeller, P. Avouris, and J. Knoch, Appl. Phys. Lett. **84**, 3693 (2004).
[6] A. Bostwick, T. Ohta, T. Seyller, K. Horn, and E. Rotenberg, Nat. Phys. **3**, 36 (2007).
[7] J.-H. Chen, C. Jang, S. Adam, M. S. Fuhrer, E. D. Williams, and M. Ishigami, Nat. Phys. **4**, 377 (2008).
[8] T. Ohta, A. Bostwick, T. Seyller, K. Horn, and E. Rotenberg, Science **313**, 951 (2006).
[9] Y. Zhang, N. W. Franklin, R. J. Chen, and H. Dai, Chem. Phys. Lett. **331**, 35 (2000).
[10] B. C. Regan, S. Aloni, R. O. Ritchie, U. Dahmen, and A. Zettl, Nature (London) **428**, 924 (2004).
[11] A. Javey, J. Guo, Q. Wang, M. Lundstrom, and H. Dai, Nature (London) **424**, 654 (2003).
[12] Z. Chen, J. Appenzeller, J. Knoch, Y.-M. Lin, and P. Avouris, Nano Lett. **5**, 1497 (2005).
[13] M. Caragiu and S. Finberg, J. Phys.: Condens. Matter **17**, R995 (2005).
[14] E. Durgun, S. Dag, S. Ciraci, and O. Gulseren, J. Phys. Chem. B **108**, 575 (2004).
[15] J. Bormet, J. Neugebauer, and M. Scheffler, Phys. Rev. B **49**, 17242 (1994).
[16] R. D. Diehl and R. McGrath, J. Phys.: Condens. Matter **9**, 951

(1997).
[17] J. P. Perdew, K. Burke, and M. Ernzerhof, Phys. Rev. Lett. **77**, 3865 (1996).
[18] G. Kresse and J. Hafner, Phys. Rev. B **47**, 558 (1993).
[19] G. Kresse and J. Hafner, Comput. Mater. Sci. **6**, 15 (1996).
[20] G. Kresse and J. Furthmüller, Phys. Rev. B **54**, 11169 (1996).
[21] P. E. Blöchl, Phys. Rev. B **50**, 17953 (1994).
[22] G. Kresse and D. Joubert, Phys. Rev. B **59**, 1758 (1999).
[23] J. C. Slater, J. Chem. Phys. **41**, 3199 (1964).
[24] G. Makov and M. C. Payne, Phys. Rev. B **51**, 4014 (1995).
[25] J. Neugebauer and M. Scheffler, Phys. Rev. B **46**, 16067 (1992).
[26] H. Jónsson, G. Mills, and K. W. Jacobsen, in *Classical and Quantum Dynamics in Condensed Phase Simulations*, edited by B. J. Berne, G. Ciccoti, and D. F. Coker (World Scientific, Singapore, 1998), p. 385.
[27] C. Kittel, *Introduction to Solid Sate Physics*, 8th ed. (Wiley, New York, 2005).
[28] F. Valencia, A. Romero, F. Ancilotto, and P. Silvestrelli, J. Phys. Chem. B **110**, 14832 (2006).
[29] S. Meng and S. Gao, J. Chem. Phys. **125**, 014708 (2006).
[30] K. Rytkönen, J. Akola, and M. Manninen, Phys. Rev. B **75**, 075401 (2007).
[31] A. Lugo-Solis and I. Vasiliev, Phys. Rev. B **76**, 235431 (2007).
[32] F. J. Ribeiro, J. B. Neaton, S. G. Louie, and M. L. Cohen, Phys. Rev. B **72**, 075302 (2005).
[33] E. Ganz, K. Sattler, and J. Clarke, Surf. Sci. **219**, 33 (1989).
[34] V. Maurice and P. Marcus, Surf. Sci. **275**, 65 (1992).
[35] S. Srivastava and J. Almöf, Surf. Sci. **274**, 113 (1992).
[36] I. Moullet, Surf. Sci. **331-333**, 697 (1995).
[37] Q. Ma and R. A. Rosenberg, Surf. Sci. **391**, L1224 (1997).
[38] Z. Zhu, G. Lu, and F. Wang, J. Phys. Chem. B **109**, 7923 (2005).
[39] P. Lindan, E. Duplock, C. Zhang, M. Thomas, R. Chatten, and A. Chadwick, Dalton Trans. **2004**, 3076.
[40] M. I. Rojas and E. P. M. Leiva, Phys. Rev. B **76**, 155415 (2007).
[41] Y. Yagi, T. M. Briere, M. H. F. Sluiter, V. Kumar, A. A. Farajian, and Y. Kawazoe, Phys. Rev. B **69**, 075414 (2004).
[42] Q. Ma and R. A. Rosenberg, Phys. Rev. B **60**, 2827 (1999).
[43] P. Jensen, X. Blase, and P. Ordejón, Surf. Sci. **564**, 173 (2004).
[44] J. Akola and H. Häkkinen, Phys. Rev. B **74**, 165404 (2006).
[45] G. M. Wang, J. J. BelBruno, S. D. Kenny, and R. Smith, Phys. Rev. B **69**, 195412 (2004).
[46] W. C. Martin and W. L. Wiese, in *Atomic, Molecular, and Optical Physics Handbook*, edited by G. W. F. Drake (American Institute of Physics, New York, 1996), pp. 135–153.
[47] Note that the magnetic moment of the ground state for the isolated Ti atom given by the GGA differs from that in experiment.
[48] F. Ancilotto and F. Toigo, Phys. Rev. B **47**, 13713 (1993).
[49] D. Lamoen and B. N. J. Persson, J. Chem. Phys. **108**, 3332 (1998).
[50] L. Lou, L. Österlund, and B. Hellsing, J. Chem. Phys. **112**, 4788 (2000).
[51] Z. Y. Li, K. M. Hock, R. E. Palmer, and J. F. Annett, J. Phys.: Condens. Matter **3**, S103 (1991).
[52] P. Bennich, C. Puglia, P. A. Brühwiler, A. Nilsson, A. J. Maxwell, A. Sandell, N. Mårtensson, and P. Rudolf, Phys. Rev. B **59**, 8292 (1999).
[53] J. Algdal, M. Breitholtz, T. Kihlgren, S.-A. Lindgren, and L. Walldén, Phys. Rev. B **73**, 165409 (2006).
[54] S. Suzuki, C. Bower, Y. Watanabe, and O. Zhou, Appl. Phys. Lett. **76**, 4007 (2000).
[55] V. Barone, J. E. Peralta, J. Uddin, and G. E. Scuseria, J. Chem. Phys. **124**, 024709 (2006).
[56] G. A. Somorjai, *Introduction to Surface Chemistry and Catalysis* (Wiley, New York, 1994).
[57] Z. Y. Li, K. M. Hock, and R. E. Palmer, Phys. Rev. Lett. **67**, 1562 (1991).
[58] K. M. Hock and R. E. Palmer, Surf. Sci. **284**, 349 (1993).
[59] L. Österlund, D. V. Chakarov, and B. Kasemo, Surf. Sci. **420**, 174 (1999).
[60] A. Kokalj, Comput. Mater. Sci. **28**, 155 (2003); http://www.xcrysden.org/